

Article

Primary Recrystallization Behaviors of Hi-B Steel with Lower Initial Nitrogen Produced by the Thin Slab Casting and Rolling Process

Bing Fu ¹, Li Xiang ^{2,*}, Jia-Long Qiao ² , Hai-Jun Wang ³, Jing Liu ¹ and Sheng-Tao Qiu ²

¹ State Key Laboratory of Refractories and Metallurgy, Wuhan University of Science and Technology, Wuhan 430081, China; fubing1986yj@163.com (B.F.); liujing@wust.edu.cn (J.L.)

² National Engineering Research Center of Continuous Casting Technology, China Iron and Steel Research Institute Group, Beijing 100081, China; qiaojialong2015@126.com (J.-L.Q.); qiustchina@126.com (S.-T.Q.)

³ School of Metallurgical Engineering, Anhui University of Technology, Ma'anshan 243002, China; whjchina@ahut.edu.cn

* Correspondence: genghao65@126.com

Abstract: Based on low-temperature high-permeability grain-oriented silicon steel designed with an initial nitrogen content of 0.0055% and produced by the thin slab casting and rolling process, the effect of total nitrogen content and nitriding temperature on primary recrystallization microstructure and texture were studied by optical microscope, scanning electron microscope, transmission electron microscope, and electron backscatter diffraction. The nitriding temperature affects the primary recrystallization behaviors significantly, while the total nitrogen content has a small effect. As the nitriding temperature is 750–850 °C, the average primary grain size and its inhomogeneity factor are about 26.58–26.67 μm and 0.568–0.572, respectively. Moreover, the texture factor is mostly between 0.15 and 0.40. Because of the relatively sufficient inhibition ability of inherent inhibitors in a decarburized sheet, the nitriding temperature (750–850 °C) affects the primary recrystallization microstructure and texture slightly. However, as the nitriding temperature rises to 900–950 °C, the average primary grain size and its inhomogeneity factor increase to 27.75–28.26 μm and 0.575–0.578, respectively. Furthermore, because of the great increase on the area fraction of {112} <110> grains, part of texture factor is increased sharply. Therefore, in order to obtain better primary grain size and homogeneity, better texture composition, and stability of the decarburized sheet, the optimal nitriding temperature is 750–850 °C.

Keywords: high permeability grain-oriented silicon steel; thin slab casting and rolling process; nitriding after decarburization; primary recrystallization; microstructure; texture



Citation: Fu, B.; Xiang, L.; Qiao, J.-L.; Wang, H.-J.; Liu, J.; Qiu, S.-T. Primary Recrystallization Behaviors of Hi-B Steel with Lower Initial Nitrogen Produced by the Thin Slab Casting and Rolling Process. *Metals* **2021**, *11*, 189. <https://doi.org/10.3390/met11020189>

Academic Editor: Matjaž Godec

Received: 16 December 2020

Accepted: 12 January 2021

Published: 21 January 2021

Publisher's Note: MDPI stays neutral with regard to jurisdictional claims in published maps and institutional affiliations.



Copyright: © 2021 by the authors. Licensee MDPI, Basel, Switzerland. This article is an open access article distributed under the terms and conditions of the Creative Commons Attribution (CC BY) license (<https://creativecommons.org/licenses/by/4.0/>).

1. Introduction

High-permeability grain-oriented silicon steel (Hi-B) is one of the most important functional materials in the development of the power industry and is widely used as a core material for transformers. At present, utilizing low-temperature slab reheating at 1100–1250 °C with the acquired inhibitor method to produce Hi-B steel has become mainstream technology. The key process is to perform short-term gas nitriding treatment on the cold rolled strip after decarburization annealing [1–5]. Nippon Steel in Japan and Bao Steel, WISCO, and Shougang Group in China have adopted this method to achieve industrial production of low-temperature Hi-B steel using the traditional process with a thick slab [4,5]. Meanwhile, the nitrogen content in the casting slab is usually controlled between 0.008% and 0.009% and a small amount of the element Sn is added as the auxiliary inhibitor. In addition, the average size of primary grains after nitriding annealing is generally limited to 20–30 μm, with the nitriding temperature mainly between 700 and 800 °C [6,7].

Compared with the traditional process, Hi-B steel produced by the thin slab casting and rolling process (TSCR) has inherent advantages in terms of energy saving, and improving production efficiency and product quality. Until recently, only AST Company in Italy, which was acquired by Thyssen Steel Company in Germany, used the compact strip production (CSP) process to manufacture Hi-B steel, and it was applied for related patents in this research field [8–12]. Furthermore, a lot of research work in this field has been carried out by NERC-CCT, WISCO, NEU, and WUST in China, and so on [13–23]. Especially, WISCO has successfully carried out the industrial production of Hi-B steel using the CSP process with the acquired inhibitor method [15].

Based on the faster solidification speed, lower soaking temperature, and shorter soaking time of a thin slab, utilizing the TSCR process is extremely beneficial in controlling the size and distribution of inherent inhibitors and in forming fine and uniform primary recrystallization grains after decarburization annealing for Hi-B steel production [13,14]. Furthermore, it will help employ a lower nitrogen content design for the composition of Hi-B steel, which makes the precise control of nitrogen in the refining process relatively easy, and the production cost will be reduced. On the other hand, it will also help employ a higher temperature at 900 °C and above during nitriding treatment, which promotes the rate of nitrogen infiltration and diffusion into the steel sheet and may directly form the required AlN inhibitor. However, it is necessary to ensure that the primary grain size is still in the appropriate range and that the grain size homogeneity is well controlled after nitriding annealing [4,6,7]. Otherwise, the stability of magnetic properties of the final product may be greatly affected. In addition, the nitriding temperature should not be too high; otherwise, the nitriding efficiency will be reduced drastically and the cost will be increased significantly.

It is well known that the primary recrystallization microstructure and texture have an extremely significant impact on the secondary recrystallization behavior and magnetic properties of Hi-B steel [4,6,7,13,14,20–23]. In order to ensure the stability of magnetic properties, the primary recrystallization microstructure and texture should have reasonable characteristics and be in an appropriate range. At present, based on utilizing the TSCR process with the acquired inhibitor method to produce Hi-B steel, the nitrogen content in thin slab is usually still 0.008% to 0.009%, and a lot of research on the nitriding treatment technology mostly focuses on one or two fixed nitriding temperatures and the formation and evolution of acquired inhibitors. However, there are a few studies on the effects of the systemic changes of nitriding temperature and total nitrogen content on the primary recrystallization behaviors under the condition of a lower initial nitrogen content in a thin slab. The characteristics and control ranges of primary recrystallization microstructure and texture after nitriding annealing are still not definite.

In this paper, a low-temperature Hi-B steel with lower initial nitrogen was manufactured by the TSCR process. The effects of the total nitrogen content and nitriding temperature on the primary recrystallization behaviors of the nitrified sheets were systematically studied, including the average grain size, the grain size inhomogeneity factor, the texture components, the texture factor, and the distribution and area fractions of specified orientation grains. Furthermore, the reasons for the changes in primary recrystallization behaviors were also investigated. It is expected to provide a reference for the production of low-temperature Hi-B steel by the TSCR process, especially for the design and optimization of the nitriding process.

2. Materials and Methods

The chemical composition (wt.%) of the experimental steel was C 0.04–0.06, Si 2.90–3.30, Mn 0.2, Cu 0.02, S 0.0047, Al_s 0.029, N 0.0055, and P 0.02. It was melted by a vacuum induction furnace and then poured into a water-cooled copper-made mold with the dimension of 50 mm × 100 mm × 400 mm. The cast slab was then transferred from the mold at a temperature higher than 950 °C to a soaking furnace, in which it was heated at 1180 °C and held for 30 min. Later, it was hot rolled to 2.55-mm-thick strips by 5 rolling

passes; the initial and final rolling temperature were 1150 °C and 920 °C, respectively. Then the hot rolled strip was cold rolled to 0.27 mm by single-stage cold-rolling after two-step normalization. Subsequently, the samples cut from cold-rolled strips were subjected to decarburization annealing at 835 °C for 3 min in a wet atmosphere of 25 vol.% H₂ + 75 vol.% N₂, and the partial pressure ratio of water vapor to hydrogen was 0.339. Then, the samples were variously nitrided from 750 to 950 °C at every 50 °C for 1 min in the mixture gas of NH₃ + H₂ + N₂, in which NH₃ was 4.8–40.3 vol.% and V_{H₂}/V_{N₂} was 3/1, to achieve different N contents. After the annealing separator mainly consisting of MgO was coated on the surfaces, the nitrided samples were subjected to secondary recrystallization annealing, which was performed in a 50 vol.% N₂ + 50 vol.% H₂ atmosphere with a heating rate of 15 °C/h up to 1210 °C and maintained for 10 h at 1210 °C under a 100% H₂ atmosphere for purification. Finally, the magnetic properties of these annealed samples with the dimension of 30 mm × 100 mm were measured by a MATS-2010SA AC magnetic measuring instrument. The magnetic induction (B₈₀₀) was measured under a magnetic field of 800 A/m, and the iron loss (P_{1.7/50}) was measured when the magnetic induction of sample was 1.7 T under 50 Hz. By injecting the appropriate N contents at different nitriding temperatures, the average measured values of the B₈₀₀ and P_{1.7/50} magnetic properties could be higher than 1.90 T and less than 1.0 W/kg, respectively [6,15].

After decarburization and nitriding, the average C and N contents in the cold-rolled sheet were measured by a carbon–sulfur analyzer and an oxygen–nitrogen analyzer, respectively. The microstructure of the nitrided sheet through thickness was observed and captured by a ZEISS-Axio Scope A1 optical microscope at 100 magnification. According to line resection in the average grain determination (GB/T 6394-2002) of metal, the average grain size \bar{X} of the microstructure of a nitrided sheet was measured. Three to four fields were randomly selected, and the number of cutoff points was about 500 in order to obtain the reasonable and accurate average value. With the help of a field emission scanning electron microscope, ZEISS SUPRA 55VP, equipped with EDAX OIM electron backscatter diffraction (EBSD), the textures of the nitrided sheet through thickness were examined and 2–4 regions in each sample were scanned with a step size of 3 μm. The software of texture, OIM analysis 6.1, was used to analyze the orientation distribution functions (ODFs), the distribution and quantitative statistics of grains with specified orientation with a maximum deviation angle of 10°.

Based on previous research methods [24–26], the relative standard deviation of grain size, that was the grain size inhomogeneity factor σ^* , was defined to quantitatively characterize the inhomogeneity of primary recrystallization grain size in a nitrided sheet. The lower the value of σ^* is, the better the homogeneity of the grain size is. The texture factor AR (area ratio) was defined to quantitatively characterize the superiority–inferiority of the textures after primary recrystallization of a nitrided sheet. AR is the ratio of the total area fractions of harmful texture to that of beneficial texture including {110} <001>. The lower the value of AR, the lower the proportion of disadvantaged texture in primary recrystallization texture and the higher the possibility of abnormal growth of a Goss-oriented grain. The calculation formulas are as follows [24–26]:

$$\sigma^* = \sigma / \mu \quad (1)$$

$$\sigma = \sqrt{\frac{1}{N} \sum_{i=1}^N (X_i - \mu)^2} \quad (2)$$

$$AR = (\{hkl\} \langle 110 \rangle + \{110\} \langle 112 \rangle) / (\{111\} \langle 112 \rangle + \{554\} \langle 225 \rangle + \{114\} \langle 481 \rangle + \{110\} \langle 001 \rangle) \quad (3)$$

where N is the quantity of grains, X_i is the size of a single grain in μm, and μ is the average size of all the grains in the total microstructure in μm. σ is the standard deviation of the grain size and is a reflection of the deviation degree of the single grain size in the total primary grain microstructure away from μ . The values of μ and σ are obtained from the grain size analysis using OIM analysis 6.1. {hkl} <110>, the α fiber texture, is the total area

fractions of $\{001\} \langle 110 \rangle$, $\{114\} \langle 110 \rangle$, $\{112\} \langle 110 \rangle$, $\{111\} \langle 110 \rangle$, $\{111\} \langle 110 \rangle$, and $\{110\} \langle 110 \rangle$; $\{111\} \langle uvw \rangle$, the γ fiber texture, is the total area fractions of $\{111\} \langle 110 \rangle$, $\{111\} \langle 112 \rangle$, and $\{554\} \langle 225 \rangle$ in this paper; and the last one is included since it is close to $\{111\} \langle 112 \rangle$.

The sample for TEM was prepared by the carbon extraction replica method. Subsequently, the morphologies of nano-precipitates in a decarburized sheet was observed by a JEOL JEM-2100F transmission electron microscope and the composition of precipitates was analyzed by energy dispersive spectrometer (EDS). Furthermore, the overall morphologies and distribution of precipitates in the decarburized sheet after electropolishing were observed by ZEISS SUPRA 55VP, and the size and density distribution of precipitates were quantitatively analyzed by using IPP (Image-Pro Plus) software. In order to ensure the accuracy of the statistical data, the sample was observed by FESEM at 20,000 magnification, and more than 30 views were collected randomly.

3. Results

3.1. Effects of Total Nitrogen Content and Nitriding Temperature on Primary Recrystallization Microstructure

After decarburization at 835 °C and nitriding at 750–950 °C, the residual carbon contents of the cold rolled sheets decrease to 0.001–0.003%, and the microstructures are ferrite grains. The typical primary recrystallization microstructures are shown in Table 1.

Table 1. Typical primary recrystallization microstructures of decarburized sheets after nitriding annealing at 750 °C and 900 °C.

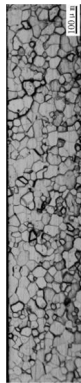
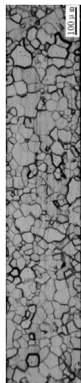
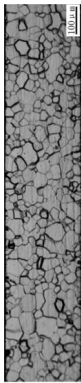
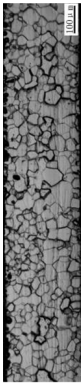
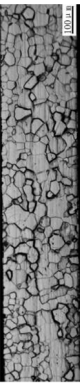
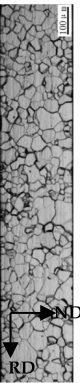
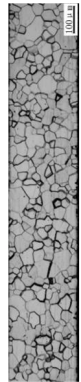
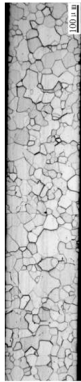
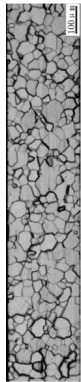
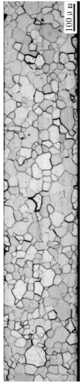
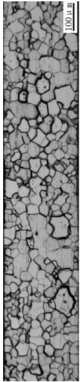
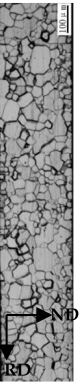
Nitriding Temperature/°C	750					
	Total Nitrogen Content/%	0.007	0.010	0.012	0.014	0.017
Microstructure						
Nitriding Temperature/°C	900					
	Total Nitrogen Content/%	0.008	0.010	0.012	0.016	0.020
Microstructure						

Figure 1 shows the relation between total nitrogen content and primary grain size and its inhomogeneity factor of a nitrified sheet at the nitrifying temperatures 750, 800, 850, 900, and 950 °C, respectively. As the total nitrogen content is in the range of 0.007–0.026%, the average grain sizes of primary recrystallization are 25.4–28.2, 25.9–27.8, 25.6–27.2, 27.1–28.6, and 27.1–28.7 μm , respectively. Meanwhile, the inhomogeneity factors are 0.55–0.58, 0.55–0.60, 0.52–0.64, 0.56–0.61, and 0.55–0.61, respectively. In other words, with the increase in total nitrogen content, the primary grain size and the inhomogeneity factor of the nitrified sheet show fluctuations. It can be considered that, under the same nitrifying temperatures, the effects of the total nitrogen content changes on the primary recrystallization microstructure are not obvious.

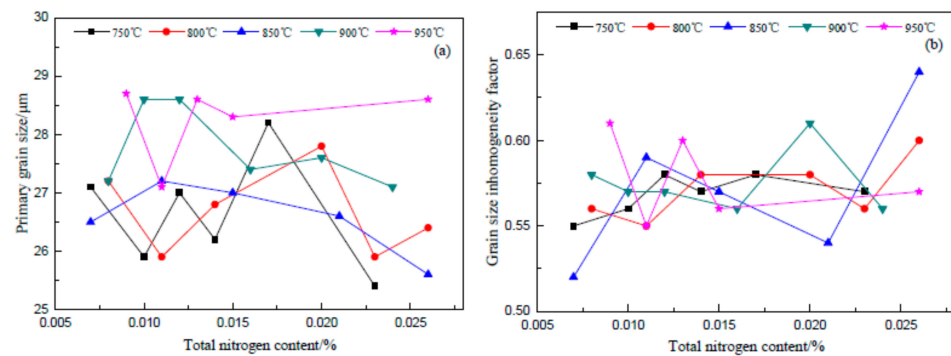


Figure 1. Relation between total nitrogen content and primary grain size (a), and the grain size inhomogeneity factor (b) of a decarburized sheet after nitrifying annealing from 750 °C to 950 °C.

It can also be seen from Figure 1 that, when the total nitrogen contents are about 0.011%, 0.014%, and 0.023%, the primary grain size increases gradually with nitrifying temperature rising from 750 °C to 950 °C. However, the inhomogeneity factor fluctuates with an increase in nitrifying temperature.

Without considering the effects of total nitrogen content changes on the primary recrystallization microstructure, the relation between the nitrifying temperature and the average values of primary grain size and its inhomogeneity factor of a nitrified sheet is shown in Figure 2. When the nitrifying temperatures are 750, 800, 850, 900, and 950 °C, the average grain sizes of primary recrystallization are 26.63, 26.67, 26.58, 27.75, and 28.26 μm and the average values of grain size inhomogeneity factor are 0.568, 0.572, 0.572, 0.575, and 0.578, respectively. These indicate that, when the nitrifying temperature is in the range of 750–850 °C, the average grain size of nitrified sheet is basically unchanged, that is, the primary grain does not grow abnormally. When the nitrifying temperature rises to 900 and 950 °C, the average grain size increases by about 1.1 and 1.6 μm , respectively, that is, the primary grain grows slightly but the abnormal growth was not obvious. In addition, when the nitrifying temperature rises from 750 to 950 °C, the average value of the grain size inhomogeneity factor in a nitrified sheet increases gradually, that is, the homogeneity of the primary recrystallization grain size deteriorates gradually. Furthermore, according to the data in Figure 1b, the maximum values of the inhomogeneity factor are relatively larger, and the fluctuation ranges are also relatively larger when the nitrifying temperature is 850–950 °C. It can be considered that, when the nitrifying temperature is higher than 850 °C, the grain size homogeneity of a nitrified sheet will become much worse.

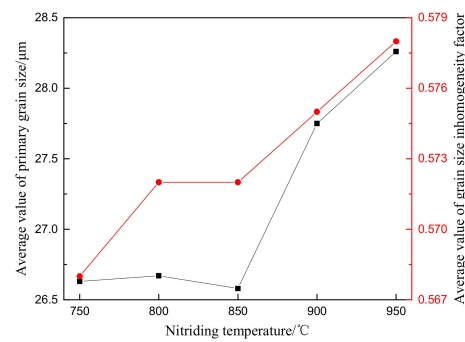


Figure 2. Relation between nitriding temperature and average values of primary grain size and its inhomogeneity factor in a nitrified sheet.

3.2. Effects of Total Nitrogen Content and Nitriding Temperature on Primary Recrystallization Texture

The ODFs for the $\varphi_2 = 45^\circ$ section through the whole thickness of typical decarburized sheets after nitriding are shown in Table 2. It can be seen that, with the increase in total nitrogen content, the primary recrystallization texture of a nitrified sheet is basically the same at the same nitriding temperatures. The texture components include strong textures for both $\{001\} \langle 120 \rangle$ and $\{114\} \langle 481 \rangle$, relatively strong γ fiber textures for $\{111\} \langle 123 \rangle$ and $\{111\} \langle 112 \rangle$, and weaker α fiber texture and much weaker textures for $\{110\} \langle 001 \rangle$, $\{110\} \langle 112 \rangle$, and $\{112\} \langle 111 \rangle$. However, the intensity of each texture component fluctuates to some extent. It can be considered that, under the condition of the same nitriding temperatures, the changes in total nitrogen content have little effect on the component and intensity of the primary recrystallization texture.

Table 2. Orientation distribution functions (ODFs) for a $\varphi_2 = 45^\circ$ section through the whole thickness of a decarburized sheet after nitriding annealing at 750 °C and 900 °C.

Nitriding Temperature/°C		750					
Total Nitrogen Content/%		0.007	0.010	0.012	0.014	0.017	0.023
	Texture level						
		max = 6.703	max = 6.485	max = 5.253	max = 5.279	max = 5.473	max = 5.545
		5.753	5.571	4.544	4.566	4.727	4.787
		4.802	4.657	3.835	3.853	3.982	4.030
		3.852	3.743	3.126	3.140	3.236	3.272
		2.901	2.828	2.418	2.426	2.491	2.515
		1.951	1.914	1.709	1.713	1.745	1.757
		1.000	1.000	1.000	1.000	1.000	1.000
		0.049	0.086	0.291	0.287	0.255	0.243
Nitriding Temperature/°C		900					
Total Nitrogen Content/%		0.008	0.010	0.012	0.016	0.020	0.024
	Texture level						
		max = 5.517	max = 4.015	max = 5.739	max = 4.105	max = 4.787	max = 6.037
		4.764	3.512	4.949	3.587	4.156	5.198
		4.012	3.010	4.159	3.070	3.525	4.358
		3.259	2.507	3.369	2.552	2.894	3.519
		2.506	2.005	2.580	2.035	2.262	2.679
		1.753	1.502	1.790	1.517	1.631	1.840
		1.000	1.000	1.000	1.000	1.000	1.000
		0.247	0.498	0.210	0.483	0.369	0.160

The distribution of specified orientation grains through the whole thickness of typical nitrified sheets is shown in Table 3. It can be seen that, with the increase in total nitrogen content, the specified orientation grains are located throughout the whole thickness of nitrified sheet at the same nitriding temperatures. That is, the distribution of specified orientation grains has no obvious rule. Moreover, the grains around most of the specified orientation grains are relatively scattered. Only the grains around Goss ($\{110\} \langle 001 \rangle$) grains exhibit obvious orientation distribution, such as for $\{114\} \langle 481 \rangle$, $\{554\} \langle 225 \rangle$, and $\{111\} \langle 112 \rangle$. It can be considered that the changes in total nitrogen content have no obvious effect on the distribution of specified orientation grains in a nitrified sheet.

Figure 3 shows the relation between the total nitrogen content and the area fractions of specified orientation grains and texture factor of nitrified sheet at the nitriding temperature of 750, 800, 850, 900, and 950 °C. It can be seen that the area fraction of the $\{114\} \langle 481 \rangle$ grain in the nitrified sheet is the highest, followed by $\{001\} \langle 120 \rangle$, γ fiber, and α fiber grains, while the area fractions of $\{110\} \langle 001 \rangle$, $\{110\} \langle 112 \rangle$, and $\{112\} \langle 111 \rangle$ grains are small. Meanwhile, the texture factor of a nitrified sheet is mostly between 0.15 and 0.40. However, the area fractions of specified orientation grains and the texture factor of a nitrified sheet show fluctuant changes with the increase in total nitrogen content at the same nitriding temperatures. It can be considered that the changes in total nitrogen content have an insignificant influence on the area fractions of specified orientation grains and the texture factor.

Table 3. The distribution of specified orientation grains through the whole thickness of a decarburized sheet after nitriding annealing at 750 °C, 850 °C, and 950 °C.

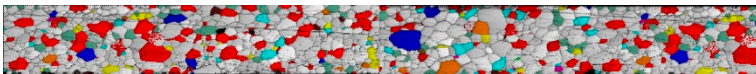
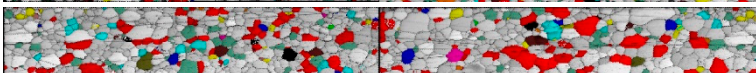
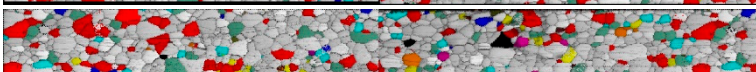
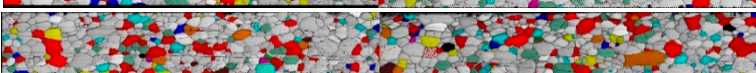
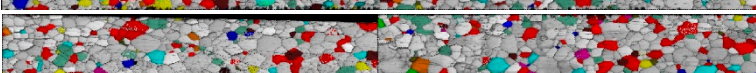
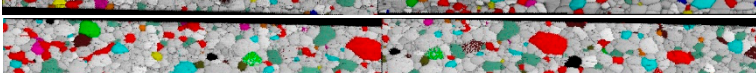
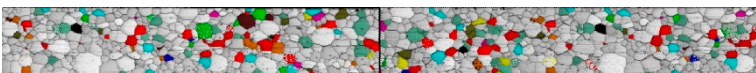
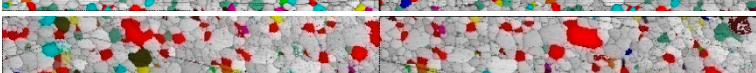
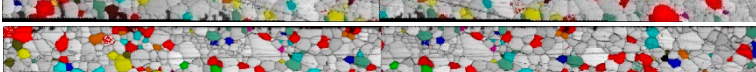
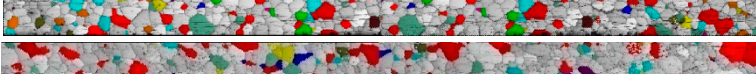
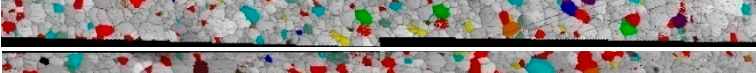
Nitriding Temperature/°C	Total Nitrogen Content/%	Distribution of Specified Orientation Grains (the Misorientation Angle is 10°)
750	0.007	
	0.010	
	0.012	
	0.014	
	0.017	
	0.023	
850	0.0074	
	0.011	
	0.015	
	0.021	
	0.026	

Table 3. Cont.

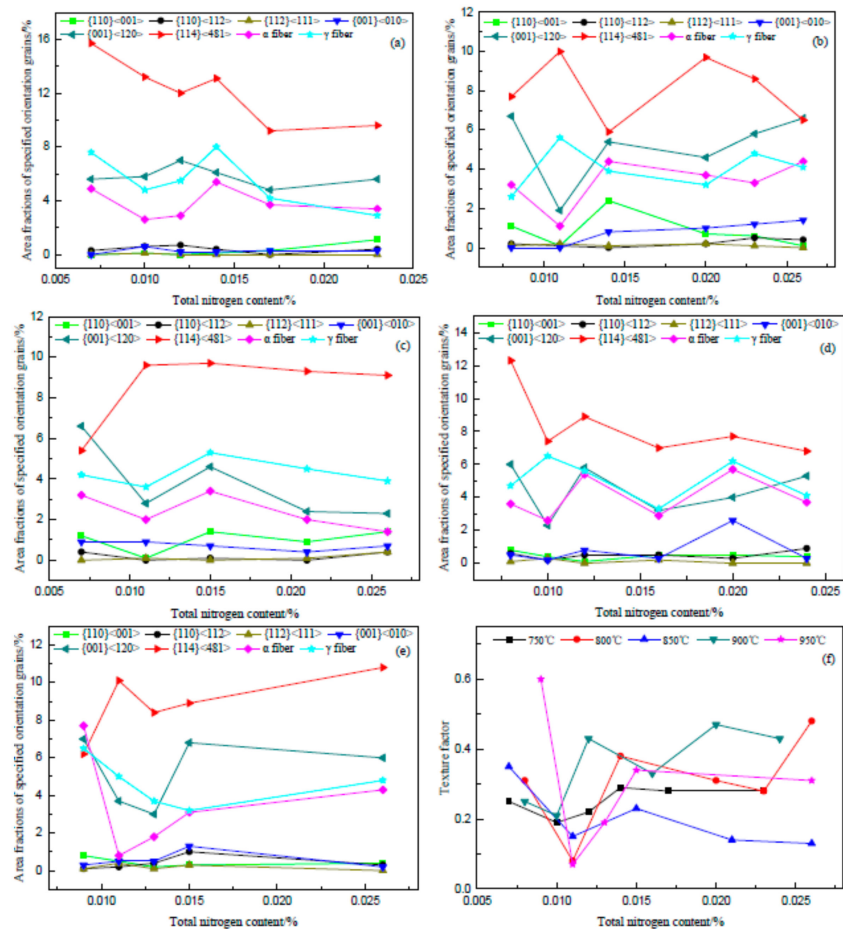
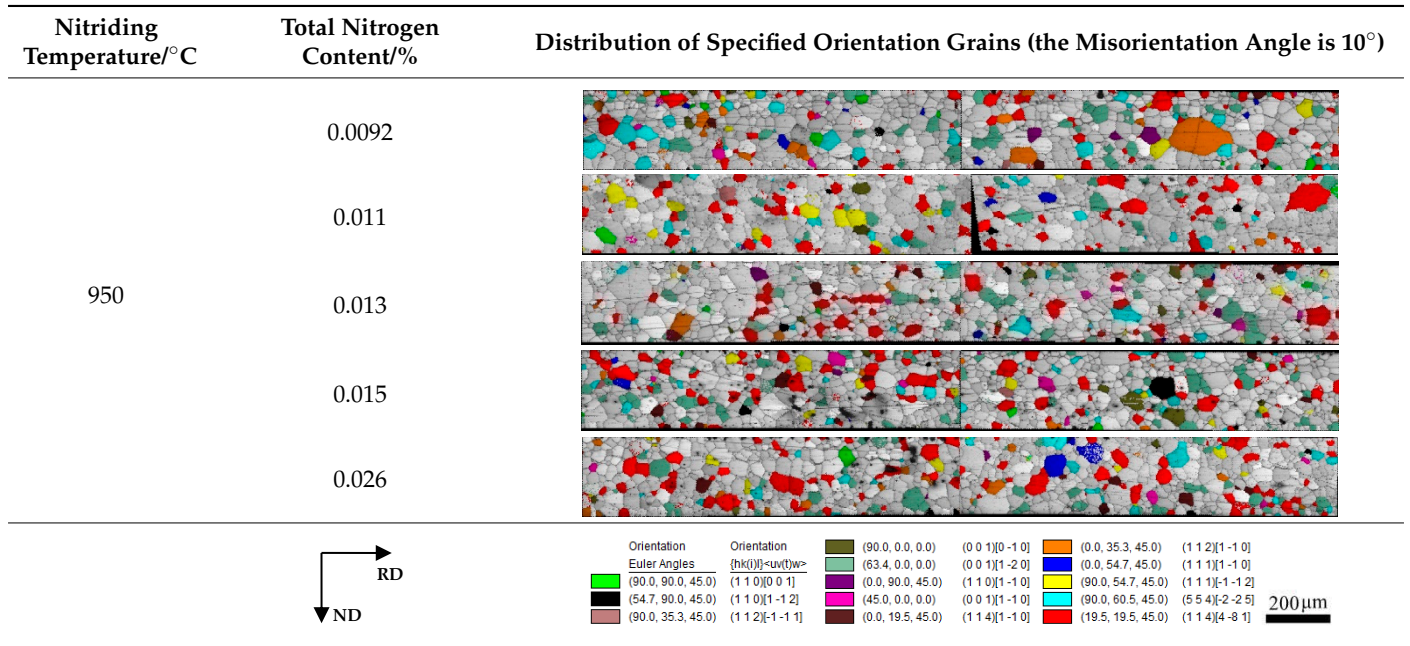


Figure 3. Relation between total nitrogen content and the area fractions of specified orientation grains and texture factor of a decarburized sheet after nitriding annealing at different temperatures: (a) 750 °C, (b) 800 °C, (c) 850 °C, (d) 900 °C, (e) 950 °C, and (f) 750–950 °C.

Similarly, according to the data in Tables 2 and 3 and Figure 3, when the total nitrogen content is about 0.011%, 0.014%, and 0.023%, respectively, with the nitriding temperature rising from 750 to 950 °C, the changes in nitriding temperature have no obvious effect on the component and intensity of the primary recrystallization texture, the distribution and area fractions of specified orientation grains, and the texture factor of a nitrided sheet.

Without considering the effects of total nitrogen content changes on the primary recrystallization texture, the relation between the nitriding temperature and average area fractions of specified orientation grains and the average value of the texture factor is shown in Figure 4. When the nitriding temperature is 750–950 °C, the average area fractions of $\{114\} \langle 481 \rangle$, $\{001\} \langle 120 \rangle$, γ fiber, and α fiber grains in nitrided sheet are in the ranges of 12.13–8.07%, 5.82–3.74%, 5.50–4.03%, and 2.40–3.98% and the average area fractions of $\{110\} \langle 001 \rangle$ and $\{110\} \langle 112 \rangle$ are 0.27–1.0% and 0.18–0.50%, respectively. Meanwhile, the average value of the texture factor of a nitrided sheet is in the range of 0.193–0.348. That is, the average area fractions of specified orientation grains in a nitrided sheet and the average value of the texture factor show fluctuant changes with the gradual increase in nitriding temperature. However, it can be seen from Figures 3f and 4 that, when the nitriding temperature is 750–850 °C, the average area fractions of $\{110\} \langle 112 \rangle$ and α fiber grains in a nitrided sheet are relatively lower, and the average value of texture factor AR is also relatively smaller. Furthermore, when the nitriding temperature is 900 and 950 °C, the texture factor is easily the maximum value (>0.4). It can be considered that, when the nitriding temperature is not higher than 850 °C, the texture components and stability of primary recrystallization in a nitrided sheet will be much better.

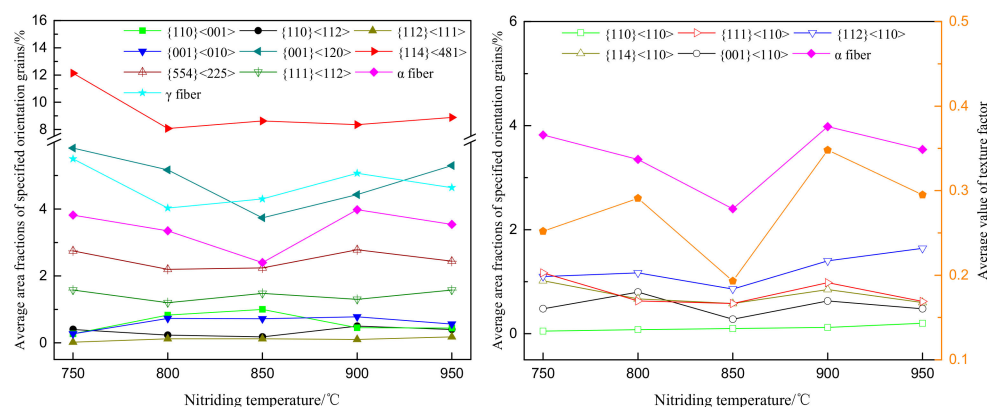


Figure 4. Relation between the nitriding temperature and average area fractions of specified orientation grains and the average value of texture factor in a nitrided sheet.

4. Discussions

It is well known that the primary grain size is mainly determined by the inhibiting ability of inherent inhibitors, that is, the precipitation state of inherent inhibitors in a decarburized sheet while the precipitation state of inherent inhibitors in Hi-B steel is dependent on steel composition and manufacturing technique before nitriding, which includes the production process, hot rolling, normalization, and decarburization annealing. The low-temperature Hi-B steel produced by the traditional process usually contains 0.008–0.009% N and makes AlN the main inherent inhibitor. However, most of the AlN precipitates during the casting process and the soaking stage of the thick slab are coarse and hardly inhibitors. In order to ensure that the primary grain size is in the appropriate range, as many fine and dispersed AlN inhibitors as possible are controlled to precipitate during the normalization and hot rolling process, especially in the cooling stage of normalizing annealing.

Because of the low N content in experimental steel, the precipitation amount of AlN inhibitors in the steel is reduced during normalization. However, the experimental steel was produced by the thin slab casting and rolling process; the faster solidification and cooling

rate, lower soaking temperature and shorter soaking time are helpful in effectively reducing the precipitation and growth of coarse nitride and sulfide and in relatively increasing the precipitation amount of fine and dispersed AlN and MnS in a thin slab [13,14]. Different from the traditional process, these are beneficial for retaining a certain number of inherent inhibitors from the slab to the decarburized sheet, which can also restrain the normal growth of primary recrystallisation grains.

The observation results by FESEM of the precipitates in a decarburized sheet are shown in Figure 5. It can be seen that there are a considerable number of dispersed precipitates in steel which precipitate in the grain interiors and grain boundaries. The size of the precipitates is generally in the range of 10–300 nm. In addition, combined with the observation results by TEM, it can be indicated that the precipitates in steel are mainly bulk nitrides and that the size is mostly 40–150 nm. The precipitation amount of spherical or spindle-shaped sulfides is relatively small, and the size is mostly 20–80 nm. Furthermore, the nitride precipitates are mainly AlN precipitated separately and include a certain amount of AlN + MnS, AlN + Cu_xS composite precipitates and a very small amount of TiN and (Al,Ti)N precipitates. The sulfide precipitates are mainly (Mn,Cu)S and (Cu,Mn)S composite precipitates and include a certain amount of MnS precipitated separately and a very small amount of Cu_xS + AlN composite precipitates. The typical morphologies and EDS results of the nitride and sulfide precipitates in a decarburized sheet are shown in Figure 6.

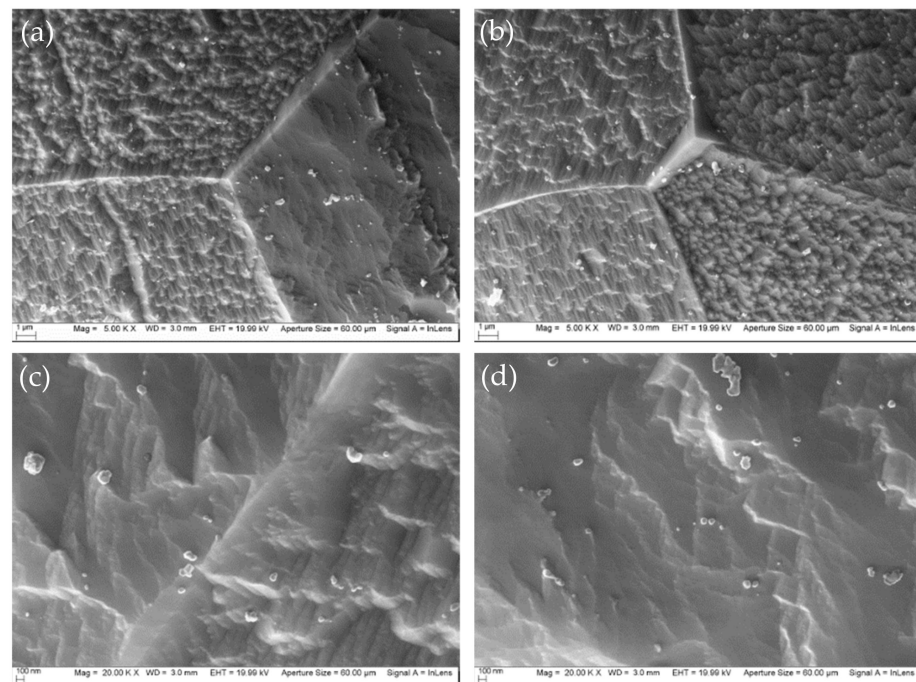


Figure 5. Distribution and morphologies of precipitates in a decarburized sheet observed by FESEM: (a,b) grain boundaries and grain interiors at 5000 magnification; (c) grain boundaries at 20,000 magnification; and (d) grain interiors at 20,000 magnification.

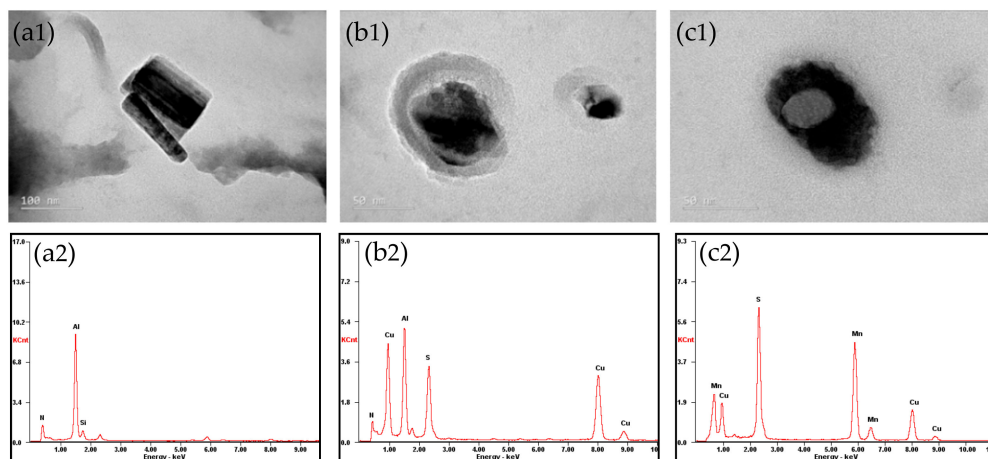


Figure 6. Typical morphologies and EDS results of precipitates in a decarburized sheet observed by TEM: (a1,a2) AlN; (b1,b2) AlN + Cu_xS; and (c1,c2) (Mn,Cu)S.

The statistical and calculated results show that the distribution density of precipitates in a decarburized sheet is $1.917 \times 10^8/\text{cm}^2$ and that the average size is about 98 nm. Meanwhile, the number of precipitates with a size distribution of 20–100 nm accounts for 59.7% of the total number, as shown in Figure 7. The distribution density of these precipitates is $1.144 \times 10^8/\text{cm}^2$, and the average size is about 61 nm. Compared with the decarburized sheet of low-temperature Hi-B steel containing 0.008–0.009% N produced by the traditional process [27,28], the size distributions of precipitates are more favorable under our experimental conditions, and the distribution density and precipitation amount of precipitates, for which the size is less than 100 nm, are significantly higher. Moreover, the primary grain size of the decarburized sheet is about 26–27 μm , which is relatively larger but still in the suitable range of 20–30 μm . These results indicate that the inhibition ability of inherent inhibitors in a decarburized sheet which can restrain the normal growth of primary recrystallisation grains may be sufficient before nitriding. Furthermore, the acquired nitride precipitates are mainly located on the surface of a decarburized sheet during nitriding treatment at 660–950 $^\circ\text{C}$ with a short time. Additionally, with the increase in nitriding temperature and time, the acquired nitride precipitates may gradually expand to the subsurface layer [7,29,30]. These acquired nitride precipitates will also play a strong effect in restraining the normal growth of primary recrystallisation grains during nitriding.

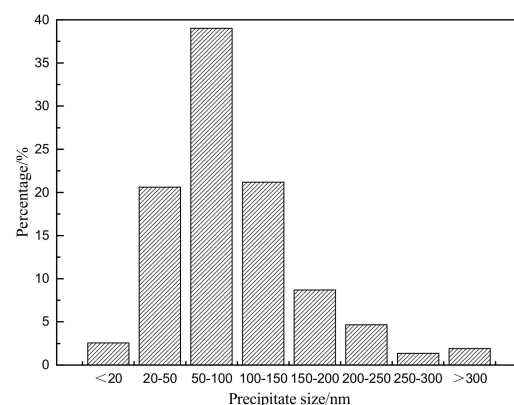


Figure 7. Size distributions of precipitates in a decarburized sheet.

When the decarburized sheet is nitrided at 750–850 $^\circ\text{C}$ for 60 s, the growth tendency of primary grains is slight during nitriding because the inhibiting ability of inherent inhibitors is sufficient and the nitriding temperature is lower. Therefore, the changes in the average value of the primary grain size and the inhomogeneity factor of a nitrided sheet are

very small. When the decarburized sheet is nitrized at 900–950 °C for 60 s, the growth tendencies of primary grains in the center layer and subsurface layer are great, since the nitrizing temperature is evidently higher than the decarburization temperature. However, because the total inhibition ability of inherent inhibitors and acquired nitride precipitates is relatively strong and the nitrizing time is short, the average value of the primary grain size is slightly increased by 1.1–1.6 μm and the grain size homogeneity of nitrized sheet is deteriorated gradually.

Under the experimental conditions, the components of primary recrystallization texture are mainly {001} <120>, {114} <481>, and γ fiber, which is consistent with the primary recrystallization texture of low-temperature Hi-B steel produced by the traditional process with the acquired inhibitor method [29–34], and the area fraction of {114} <481> grains is much higher than {001} <120> and γ fiber grains in a nitrized sheet, which is consistent with the research result of Li, X. and Yasuda, M. but partly different from that of Liu, G.T. [30–32]. During the process of decarburization and nitrizing annealing, the characteristics and changes in texture of the nitrized sheet are closely related to the formation and changes in its microstructure. It is generally believed that, during grain growth after recrystallization is completed in the cold-rolled sheet, the α fiber texture will be obviously gathered at the {114} <481> orientation, which makes the texture intensity and area fraction of {114} <481> grains increase greatly. However, the texture intensity and area fraction of {111} <112> grains will be reduced obviously. Moreover, with the substantial increase in annealing temperature or time during primary recrystallization, that is, with the obvious growth in primary grain size, the texture intensity and area fraction of {114} <481> grains will also be increased significantly [31–34].

When the decarburized sheet is nitrized at 750–850 °C for 60 s, because the changes in the average value of primary grain size and the inhomogeneity factor of a nitrized sheet are very small, the main features of the primary recrystallization texture have not changed. Both the average area fractions of specified orientation grains in a nitrized sheet and the average value of texture factor remain unchanged or have a certain range of fluctuations. When the decarburized sheet is nitrized at 900–950 °C for 60 s, because the average value of primary grain size and its inhomogeneity factor is only increased to some extent, the textures intensity and area fractions of {114} <481>, {111} <112>, and {554} <225> grains in nitrized sheet are not increased significantly but only fluctuate in a certain range at whole nitrizing temperatures. However, since the area fraction of {112} <110> grains increased significantly from 0.86–1.17% to 1.40–1.64% and a small amount of these grains grew obviously, seen in Figure 4 and Table 3, the average value of the texture factor shows some increase and the texture factors of some nitrized sheets obtain maximum values. The growth mechanism of {112} <110> orientation grains and its influencing factors during nitrizing at higher temperatures still need to be further studied. In summary, in order to ensure that the decarburized sheet has better primary grain size and homogeneity, better texture composition, and stability, the nitrizing temperature should be controlled at 750–850 °C under our experimental conditions.

5. Conclusions

- (1) After the decarburized sheet was nitrized at 750–950 °C, the average primary grain size and its inhomogeneity factor were in the range of 26.58–28.26 μm and 0.568–0.578, respectively. The components of primary recrystallization texture were mainly {001} <120>, {114} <481>, and γ fiber texture. Meanwhile, the area fraction of {114} <481> grains in the nitrized sheet was the highest, followed by {001} <120>, γ fiber, and α fiber grains, and the texture factor was mostly between 0.15 and 0.40.
- (2) At the same nitrizing temperatures, the effects of the total nitrogen content on both the primary grain size and the inhomogeneity factor of a nitrized sheet were not obvious. The effects of total nitrogen content on the component and intensity of primary recrystallization texture, the distribution and area fractions of specified orientation grains, and the texture factor of nitrized sheet were also insignificant.

- (3) When the nitriding temperature was 750–850 °C, because the inhibition ability of inherent inhibitors in a decarburized sheet was relatively sufficient, the changes in nitriding temperature have little effect on the primary recrystallization microstructure and texture. When the nitriding temperature rose to 900–950 °C, the average value of primary grain size increased by 1.1–1.6 μm and the inhomogeneity factor also increased gradually. Moreover, some values of the texture factor increased sharply because of the area fraction of {112} <110> grains increased greatly in the nitrified sheet. In order to ensure that the decarburized sheet had better primary recrystallization microstructure and texture characteristics, the nitriding temperature should be controlled between 750 and 850 °C.

Author Contributions: Conceptualization, B.F. and L.X.; methodology, B.F.; software, J.-L.Q.; validation, B.F., L.X., and H.-J.W.; formal analysis, B.F.; investigation, B.F.; resources, B.F.; data curation, B.F.; writing—Original draft preparation, B.F.; writing—Review and editing, B.F. and J.L.; visualization, J.L.; supervision, L.X.; project administration, S.-T.Q.; funding acquisition, S.-T.Q. All authors have read and agreed to the published version of the manuscript.

Funding: This work was financially supported by the National Key Research and Development Program of China (2016YFB0300305).

Data Availability Statement: Data available in a publicly accessible repository.

Conflicts of Interest: The authors declare no conflict of interest.

References

1. Takahashi, N.; Suga, Y.; Kobayashi, H. Recent developments in grain-oriented silicon steel. *J. Magn. Magn. Mater.* **1996**, *160*, 98–101. [[CrossRef](#)]
2. Kubota, T.; Fujikura, M.; Ushigami, Y. Recent progress and future trend on grain-oriented silicon steel. *J. Magn. Magn. Mater.* **2000**, *215–216*, 69–73. [[CrossRef](#)]
3. Xia, Z.S.; Kang, Y.L.; Wang, Q.L. Developments in the production of grain-oriented electrical steel. *J. Magn. Magn. Mater.* **2008**, *320*, 3229–3233. [[CrossRef](#)]
4. Qiu, S.T.; Fu, B.; Xiang, L.; Cheng, G.G. Recent research trends and developments of production process and technology for high magnetic induction grain-oriented silicon steel. *Iron Steel.* **2013**, *48*, 1–8.
5. Li, X.H.; Meng, X.T.; Zhao, P.F.; He, X.G.; Yu, H.B.; Luo, H.W. Present status and future prospect of high permeability grain-oriented silicon steel. *China Metall.* **2019**, *29*, 1–7.
6. Fu, B.; Xiang, L.; Qiu, S.T.; Cheng, G.G. Research advances in inhibitors control of low-temperature high magnetic induction grain-oriented silicon steel production with acquired inhibitor method. *Chin. J. Process Eng.* **2014**, *14*, 173–180.
7. Luo, X.G.; Guo, X.L.; Gao, Y.; Chen, W.C.; Ding, Z. Effect of nitriding temperature on the inhibitor state of grain-oriented silicon steel. *J. Wuhan Univ. Sci. Technol.* **2019**, *42*, 8–12.
8. Fortunati, S.; Cicale, S.; Abbruzzese, G. Process for the Production of Grain Oriented Electrical Steel Strip Having High Magnetic Characteristics, Starting from Thin Slabs. U.S. Patent 6,296,719B1, 2 October 2001.
9. Cicale, S.; Fortunati, S.; Abbruzzese, G. Process for the Inhibition Control in the Production of Grain-Oriented Electrical Sheets. U.S. Patent 6,361,620B1, 26 March 2002.
10. Fortunati, S.; Cicale, S.; Abbruzzese, G. Process for the Inhibition Control in the Production of Grain-Oriented Electrical Sheets. U.S. Patent 6,361,621B1, 26 March 2002.
11. Fortunati, S.; Cicale, S.; Abbruzzese, G.; Matera, S. Process for the Treatment of Grain Oriented Silicon Steel. U.S. Patent 6,406,557B1, 18 June 2002.
12. Günther, K.; Lahn, L.; Ploch, A.; Sowka, E. Method for Producing Grain Oriented Magnetic Steel Strip. U.S. Patent 8,088,229B2, 3 January 2012.
13. Qiu, S.T.; Xiang, L.; Yue, E.B.; Zhao, P. Technology analysis of producing grain oriented silicon steel by thin slab casting and rolling process. *Iron Steel* **2008**, *43*, 1–7.
14. Fu, B.; Xiang, L.; Qiu, S.T.; Cheng, G.G. Research status and technological analysis of producing high magnetic induction grain-oriented silicon steel by thin slab casting and rolling process. *Mater. Rev.* **2013**, *27*, 110–114.
15. Xiang, L.; Chen, S.L.; Pei, Y.H.; Luo, Z.H.; Qiu, S.T. Domestic current status and research progress of producing electrical steel by thin slab casting and rolling process. In Proceedings of the 11th China Steel Congress, Beijing, China, 21–22 November 2017; pp. 69–74.
16. Chen, S.L.; Fang, Z.M.; Luo, Z.H.; Wu, J.P.; Sun, L.; Wang, C.F.; Huang, B.; Guo, X.L.; Zhang, C.; Liang, Z.R.; et al. Method for Producing High Permeability Grain Oriented Silicon Steel by Thin Slab Casting and Rolling. China Patent CN102,517,429A, 27 June 2012.

17. Yu, Y.M.; Xu, Y.B.; Li, C.S.; Wang, G.D. Inhibitor precipitation of Fe-3% Si strip by thin slab casting and rolling. *Trans. Mater. Heat Treat.* **2010**, *31*, 21–25.
18. Li, C.S.; Yang, H.; Wang, Y.F.; Yu, Y.M. Texture of hot rolled strip for Fe-3Si steel produced by thin slab casting and rolling. *J. Iron Steel Res. Int.* **2010**, *17*, 46–53. [[CrossRef](#)]
19. Bao, S.Q.; Xu, Y.; Zhao, G.; Huang, X.B.; Xiao, H.; Ye, C.L.; Song, N.N.; Chang, Q.M. Microstructure, texture and precipitates of grain-oriented silicon steel produced by thin slab casting and rolling process. *J. Iron Steel Res. Int.* **2017**, *24*, 91–96. [[CrossRef](#)]
20. Huang, F.Y.; Zhao, G.; Xu, Y.; Su, C.Q. Influence of inhibitors on primary recrystallization structure of Hi-B electrical steel. *J. Iron Steel Res.* **2018**, *30*, 373–378.
21. Su, C.Q.; Zhao, G.; Xiao, H.; Lan, Y.Z.; Huang, F.Y. Abnormal grain growth of Hi-B steel in the secondary recrystallization. *Metallogr. Microstruct. Anal.* **2018**, *7*, 608–617. [[CrossRef](#)]
22. Bao, S.Q.; Liu, B.B.; Zhao, G.; Lan, Y.Z.; Huang, F.Y. Secondary recrystallisation behaviours of grain-oriented silicon steel produced by TSCR process. *Ironmak. Steelmak.* **2018**, *45*, 924–928. [[CrossRef](#)]
23. Huang, F.Y.; Bao, S.Q.; Zhao, G.; Su, C.Q. Effect of different nitriding temperature on secondary recrystallization of Hi-B steel with an element of Cu. *Metallogr. Microstruct. Anal.* **2019**, *8*, 12–22. [[CrossRef](#)]
24. Fu, B.; Xiang, L.; Wang, H.J.; Qiu, S.T. Effects of nitrogen content and nitriding temperature on primary recrystallization behaviors of high magnetic induction grain-oriented silicon steel. In Proceedings of the Seminar Conference on Production Technology and Application of Domestic High-performance Electrical Steel, Dalian, China, 25–26 August 2016; pp. 22–34.
25. Wang, H.J.; Fu, B.; Xiang, L.; Rong, Z.; Qiu, S.T. Effect of nitrogen content on primary recrystallization behavior and magnetic property of Hi-B steel. *J. Iron Steel Res. Int.* **2016**, *23*, 1080–1085. [[CrossRef](#)]
26. Xiang, L.; Rong, Z.; Fu, B.; Wang, H.J.; Qiu, S.T. Characterizing microstructure and texture after recrystallization annealing of hi-b steel with simultaneous decarburization and nitriding. *J. Iron Steel Res. Int.* **2017**, *24*, 1215–1222. [[CrossRef](#)]
27. Wu, Z.W.; Li, J.; Zhao, Y.; Li, B. Low-temperature heating technology oriented silicon steel decarburization and nitriding process and organization. In Proceedings of the 11th China Electrical Steel Professional Academic Annual Conference, Xiamen, China, 9–12 December 2010; pp. 172–176.
28. Wu, Z.W.; Zhao, Y.; Li, J.; Li, B. Study on precipitates of grain-oriented silicon steel produced by acquired inhibitor method. *J. Mater. Eng.* **2012**, *2*, 55–58.
29. Wang, R.; Yang, P.; Liu, G.T. Effect of nitriding temperature on inhibitor precipitation and the annealed microstructure of grain-oriented silicon steel produced by acquired inhibitor method. *Chin. J. Stereol. Image Anal.* **2016**, *21*, 272–278.
30. Li, X.; Yang, P.; Jia, Z.W.; Zhang, H.L. Effects of normalizing process and nitriding process on the microstructure, texture, and magnetic properties in low-temperature grain-oriented silicon steel. *Chin. J. Eng.* **2019**, *41*, 610–617.
31. Yasuda, M.; Kataoka, T.; Ushigami, Y.; Murakami, K.; Ushioda, K. texture evolution during recrystallization and grain growth in heavily cold-rolled Fe-3%Si alloy. *ISIJ Int.* **2018**, *58*, 1893–1900. [[CrossRef](#)]
32. Liu, G.T.; Liu, Z.Q.; Yang, P.; Mao, W.M. Correlation between primary and secondary recrystallization texture components in low-temperature reheated grain-oriented silicon steel. *J. Iron Steel Res. Int.* **2016**, *23*, 1234–1242. [[CrossRef](#)]
33. Liu, G.T.; Liu, Z.Q.; Yang, P.; Mao, W.M. Effect of primary recrystallized microstructure and nitriding on secondary recrystallization in grain oriented silicon steel by low temperature slab reheating. *J. Mater. Eng.* **2018**, *46*, 16–24.
34. Liu, Z.Q.; Yang, P.; Mao, W.M.; Cui, F.E. Effect of {114} <418> texture on abnormal growth during secondary recrystallization in grain-oriented steel. *Acta Metall. Sin.* **2015**, *51*, 769–776.